Archival Report

Biological Psychiatry

Opposing Effects on $Na_V1.2$ Function Underlie Differences Between *SCN2A* Variants Observed in Individuals With Autism Spectrum Disorder or Infantile Seizures

Roy Ben-Shalom, Caroline M. Keeshen, Kiara N. Berrios, Joon Y. An, Stephan J. Sanders, and Kevin J. Bender

ABSTRACT

BACKGROUND: Variants in the *SCN2A* gene that disrupt the encoded neuronal sodium channel $Na_V1.2$ are important risk factors for autism spectrum disorder (ASD), developmental delay, and infantile seizures. Variants observed in infantile seizures are predominantly missense, leading to a gain of function and increased neuronal excitability. How variants associated with ASD affect $Na_V1.2$ function and neuronal excitability are unclear.

METHODS: We examined the properties of 11 ASD-associated *SCN2A* variants in heterologous expression systems using whole-cell voltage-clamp electrophysiology and immunohistochemistry. Resultant data were incorporated into computational models of developing and mature cortical pyramidal cells that express $Na_V1.2$.

RESULTS: In contrast to gain of function variants that contribute to seizure, we found that all ASD-associated variants dampened or eliminated channel function. Incorporating these electrophysiological results into a compartmental model of developing excitatory neurons demonstrated that all ASD variants, regardless of their mechanism of action, resulted in deficits in neuronal excitability. Corresponding analysis of mature neurons predicted minimal change in neuronal excitability.

CONCLUSIONS: This functional characterization thus identifies *SCN2A* mutation and $Na_V1.2$ dysfunction as the most frequently observed ASD risk factor detectable by exome sequencing and suggests that associated changes in neuronal excitability, particularly in developing neurons, may contribute to ASD etiology.

Keywords: Autism spectrum disorder, Epilepsy, $Na_V1.2$, electrophysiology, *SCN2A*, Seizure

http://dx.doi.org/10.1016/j.biopsych.2017.01.009

Exome sequencing has transformed gene discovery in autism spectrum disorder (ASD). Observing multiple de novo protein-truncating variants (PTVs) (e.g., premature stop codons) in a gene demonstrates ASD association (1), and to date, 65 such ASD genes have been identified (2–4). The gene *SCN2A*, which encodes the sodium channel $Na_V1.2$, was one of the first ASD genes identified (1) and remains one of the genes with the strongest evidence for association with ASD (2) and, recently, developmental delay (5). *SCN2A* stands out from other ASD-associated genes in several ways. First, while most ASD-associated genes are related to either chromatin regulation or synapse structure (2), $Na_V1.2$ channels are primarily expressed in the axon (6–10). Second, along with de novo PTVs, an excess of de novo missense mutations is also observed in *SCN2A*, a pattern seen in no other gene (2). Finally, genetic variants in *SCN2A* have previously been associated with infantile seizures, ranging from benign infantile familial seizures (BIFS) to epileptic encephalopathy (EE) with poor developmental outcome (11); however, only 4 of 19 ASD patients for whom phenotypic data were available had a history of seizures and none had infantile seizures (Table S1 in Supplement 2).

$Na_V1.2$ channels support central functions in developing and mature neurons, particularly in cortical glutamatergic pyramidal cells (6,7) that are a locus of dysfunction in ASD (12–14). During early development, $Na_V1.2$ is the only Na_V isoform expressed at nodes of Ranvier and in the axon initial segment (AIS) (15–17), the site of action potential (AP) initiation in most neurons (18,19). $Na_V1.2$ is therefore critical for AP generation and propagation because these neurons integrate into circuits. Later in development $Na_V1.2$ is replaced by $Na_V1.6$ (*SCN8A*), which has a lower voltage threshold for activation at the majority of nodes and in the distal AIS (7,10). Consequently, AP initiation occurs in this $Na_V1.6$-rich region in mature neurons (19,20), and $Na_V1.2$, now restricted to the proximal AIS, takes on a new role, boosting rather than initiating APs (6). This developmental transition in AIS distribution may explain the resolution of seizures observed in BIFS before 2 years of age (13).

The majority of *SCN2A* missense variants associated with infantile seizures in BIFS and EE are gain of function [(7,21–25),

ISSN: 0006-3223

but see (26)]. In contrast, mutations observed in ASD/developmental delay are either PTVs resulting in loss of $Na_V1.2$ function or missense mutations of unknown effect. These observations raise the hypothesis that *SCN2A* variants exert opposing effects on $Na_V1.2$ function in infantile seizures and ASD.

Here, we used bioinformatics, electrophysiology, and compartmental modeling to test how different *SCN2A* variants affect the function of $Na_V1.2$ channels. We report that the majority of missense mutations observed in ASD completely blocked channel conductance, while the remainder altered $Na_V1.2$ biophysical properties in ways that dampened channel function. Regardless of mechanism, all ASD-related variants impaired neuronal excitability in computational models of developing pyramidal cells. These impairments largely resolved because $Na_V1.6$ replaced $Na_V1.2$ in the distal AIS of mature models, supporting the notion that ASD is a consequence of disruption to early brain development leading to persistent neurodevelopmental dysfunction (27). Results from these de novo missense mutations in 8 individuals, along with 4 individuals with de novo PTVs, identify *SCN2A* mutations in 0.3% of ASD cases (12 of 4109 cases with exome data). *SCN2A* therefore has the strongest evidence of ASD association of any gene discovered by exome sequencing and is the most frequent single gene contributor to ASD, after fragile X mutations.

METHODS AND MATERIALS

Briefly, wild-type (WT) and variants of *SCN2A* harboring an ASD-associated mutation were cotransfected with β1-β2 subunits in HEK293 cells. Sodium channel function was assessed with voltage-clamp techniques and immunohistochemistry, and then incorporated into a pyramidal cell computational model. Please see Supplemental Methods in Supplement 1 for details.

RESULTS

A comprehensive literature review identified 148 *SCN2A* variants (117 unique) in 148 families (Table S1 in Supplement 2). Building on the description by Howell *et al.* (11), variants clustered in four phenotypic groups: 20 variants in families with BIFS; 8 variants in individuals with infantile seizures and mild developmental delay and/or episodic ataxia; 51 variants in individuals with EE characterized by infantile seizures and moderate to severe developmental delay, often accompanied by central hypotonia, cerebral atrophy, and microcephaly; and 39 variants in individuals with a developmental disorder characterized by ASD and/or intellectual disability. This latter group includes a few individuals with comorbid seizures with onset after the age of 1.5 years, a frequent occurrence in both ASD and developmental delay. A further 16 variants lack sufficient phenotypic information to assign them to one of these four groups, while 15 variants do not clearly match these groups (e.g., febrile seizures, herpes encephalitis, schizophrenia).

Of the 20 variants observed in BIFS, 19 (95%) are missense variants and 1 is a 507 kbp duplication; 18 (90%) of the variants are inherited with the variant segregating with phenotype in multiple affected family members. BIFS missense variants cluster in the transmembrane segments and short connecting loops (16 of 19 variants; 2.3-fold over expectation; $p = .0004$, binomial test; Figure 1A), particularly in and between transmembrane segments 4 and 5 that are proximal to the voltage sensor (11 of 19 variants; 4.7-fold over expectation; $p = 4 \times 10^{-5}$, binomial test; Figure 1A).

Similarly, variants observed in EE are mainly missense variants (49 of 51 variants, 96%) along with one 2.6 Mbp duplication and one PTV; however, unlike BIFS variants, most are de novo (48 of 49 variants with inheritance data, 98%). EE missense variants also cluster in and between the transmembrane segments (39 of 49 variants; twofold enrichment; $p = 2 \times 10^{-6}$, binomial test; Figure 1A), particularly segments 4 and 5 (24 of 49 variants; fourfold enrichment; $p = 4 \times 10^{-10}$, binomial test; Figure 1A). While the variants in BIFS and EE cluster in similar domains of the $Na_V1.2$ protein, there are no examples of a variant contributing to both disorders, despite multiple recurrent variants in different families being observed in both BIFS (4xR1319Q) and EE (4xR853Q, 3xE999K, 3xL1342P, 3xR1882Q). Seven BIFS and three EE variants have been characterized electrophysiologically (Tables S1 and S2 in Supplement 2), largely revealing gain of function thought to result in neuronal hyperexcitability [(7,21–25); but see (26)].

In contrast to BIFS and EE, over half of the ASD-associated variants are predicted to prevent translation of one *SCN2A* allele, with 12 PTVs and two deletions (14 of 27 variants, 52%). Exome Aggregation Consortium (28) and Residual Variation Intolerance Score (29), two methods that use large-scale population data to identify constrained genes that are intolerant of deleterious variation, both predict that *SCN2A* is highly intolerant of such haploinsufficiency, with 30-fold fewer PTVs observed in an adult population than was expected. Consistent with a highly deleterious effect, all PTVs and deletion variants are de novo (13 of 13 variants for which data are available; Table S1 in Supplement 2). The remaining 13 (48%) variants in ASD cases are missense (Table S1 in Supplement 2), and most of these are also de novo (12 of 13 variants, 92%). Unlike the missense variants in BIFS and EE, ASD-missense variants cluster in the pore loop that forms the sodium ion selectivity filter (8 of 13 variants; 3.8-fold enrichment; $p = .0004$ binomial test; Figure 1B, C), particularly in the five amino acid residues that line the pore upstream of the ion selectivity filter (3) (6 of 13 variants; 33-fold enrichment; $p = 1 \times 10^{-8}$ binomial test; Figure 1C). Many individuals with ASD have coexisting intellectual disability (Figure 1D) and developmental delay (Table S1 in Supplement 2). Accordingly, the 12 variants in *SCN2A* in individuals with developmental delay, but no known diagnosis of ASD, are mostly PTVs (8 of 12 variants, 67%) and de novo (11 of 12 variants, 92%).

This raises the hypothesis that *SCN2A* variants resulting in $Na_V1.2$ gain of function and increased neuron excitability lead to infantile seizures, whereas *SCN2A* variants resulting in $Na_V1.2$ loss of function and decreased neuron excitability lead to ASD and/or developmental delay. If this hypothesis were correct, we would expect the missense variants observed in ASD to reduce $Na_V1.2$ channel function and decrease neuron excitability. We therefore performed functional analyses of all 12 de novo *SCN2A* mutations observed in the 4109 ASD cases from the Simons Simplex Collection (2508 families with

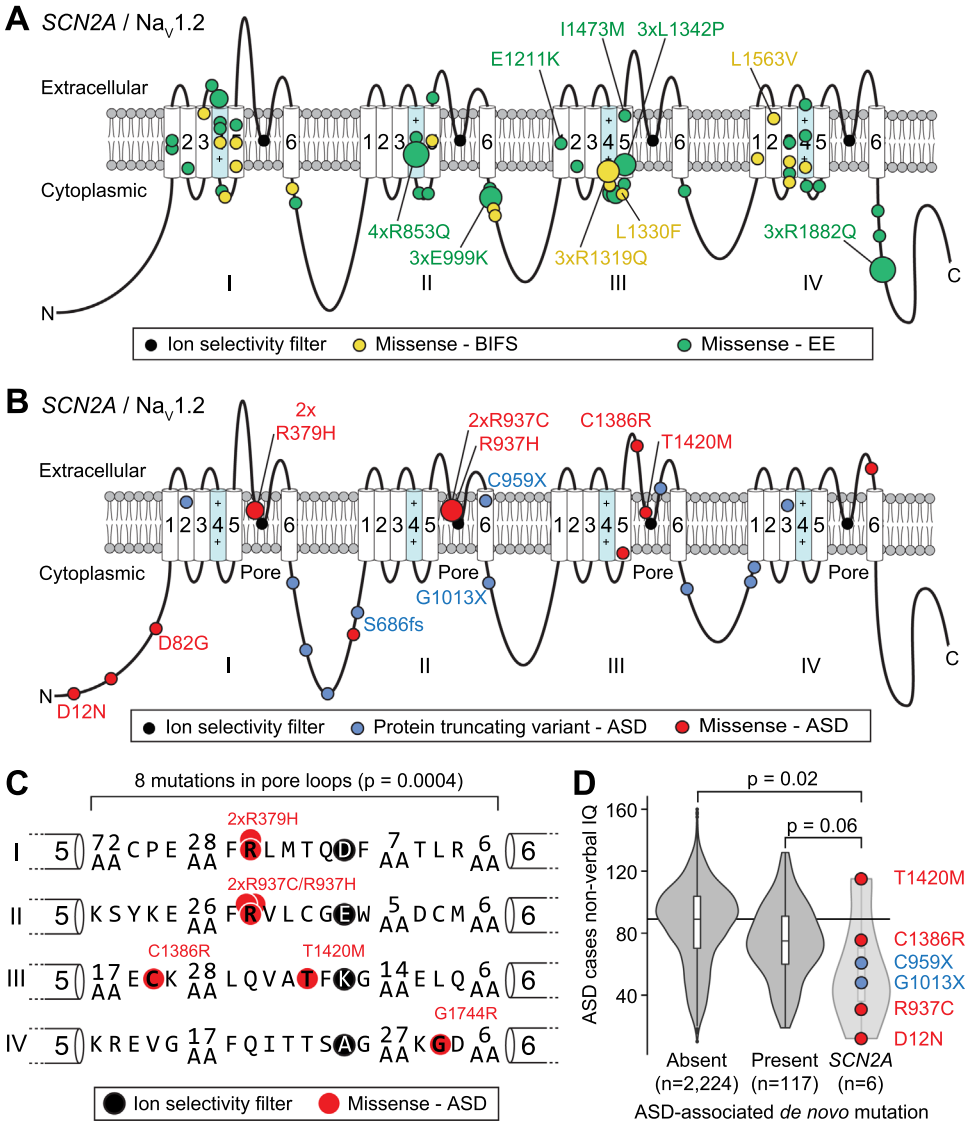

Figure 1. *SCN2A*/$Na_V1.2$ genotypes and phenotypes. **(A)** Location of 19 missense *SCN2A* variants in benign infantile familial seizures (BIFS) (yellow) and 49 missense *SCN2A* variants in epileptic encephalopathy (EE) (green) in the $Na_V1.2$ sodium channel. The size of the circle corresponds to the number of individuals with a variant at a specific residue. Variants that are observed in three or more independent families are named, with the text color corresponding to the phenotype. **(B)** Location of 13 missense (red) and 10 protein-truncating variants (PTVs) (blue) *SCN2A* variants in autism spectrum disorder (ASD) cases in the $Na_V1.2$ sodium channel. The size of the circle corresponds to the number of individuals with a variant at a specific residue. Variants that were functionally assessed are named, with the text color corresponding to the variant type. **(C)** A zoomed in view of the eight missense *SCN2A* variants on the pore loop observed in ASD. Six of these variants are within five amino acid (AA) residues of the ion selectivity filter. Statistical significance was calculated using a two-sided binomial exact test. **(D)** A violin plot of nonverbal IQ in 2347 ASD cases from the Simons Simplex Collection; equivalent data are not available for the Autism Sequencing Consortium cases. The overlaid boxplot shows the median and interquartile range. The cases are divided into three groups: 2224 with no known de novo PTV, deletion, or duplication mutations; 117 with a de novo PTV, deletion, or duplication in an ASD-associated gene or locus (2); 6 with a de novo PTV (blue) or missense (red) mutation in *SCN2A*. Statistical significance was calculated using a two-sided Wilcoxon signed rank test.

a single affected child) and Autism Sequencing Consortium (1601 families with one or more affected children), as these cases were identified as representing idiopathic ASD in clearly defined cohorts (4,9,22).

To confirm that PTV *SCN2A* mutations indeed impair $Na_V1.2$ channel formation, and to determine whether missense mutations alter channel function, we made voltage-clamp recordings from HEK293 cells expressing WT or mutated channels. β1 and β2 subunits were coexpressed in all experiments. As predicted, nonsense (p.C959X, p.G1013X) and frameshift (p.S686fs) PTVs lacked Na^+ currents (Figure 2A, B). Constructs recapitulating a fourth PTV that disrupts a canonical splice site in *SCN2A* (c.4821-1A>T) were not studied here, as it was unclear whether the messenger RNA recombines after this splice event. The missense mutations produced a range of results. Peak currents from D12N-mutated channels were comparable in size to WT (WT: −447 ± 45 pA/pF, $n = 18$; D12N: −515 ± 65 pA/pF, $n = 16$; $p = .5$), while currents from D82G and T1420M variants were smaller than those from WT channels (D82G: −166 ± 32 pA/pF, $n = 18$, $p < .0001$ vs. WT; T1420M: −177 ± 22 pA/pF, $n = 13$, $p < .0001$ vs. WT). Remarkably, all other missense mutations, including pore-localized arginine mutations observed in multiple ASD cases (R379, R937), resulted in a loss of $Na_V1.2$ function. Small residual currents were observed, but these were likely generated by endogenously expressed nonselective cation channels (30), as they were observed in all PTV cases (where no channel was formed but the plasmid vector still expressed green fluorescent protein) and in untransfected cells (Figure 2B). Furthermore, no current was observed when using a K^+-based intracellular solution, indicating that these channels are not permeable to K^+. Despite the lack of current, nonconducting missense mutations still allowed for $Na_V1.2$ channel formation and trafficking, as membrane-associated $Na_V1.2$ staining was evident using confocal and total internal reflectance fluorescence microscopy (Figure S2 in Supplement 1).

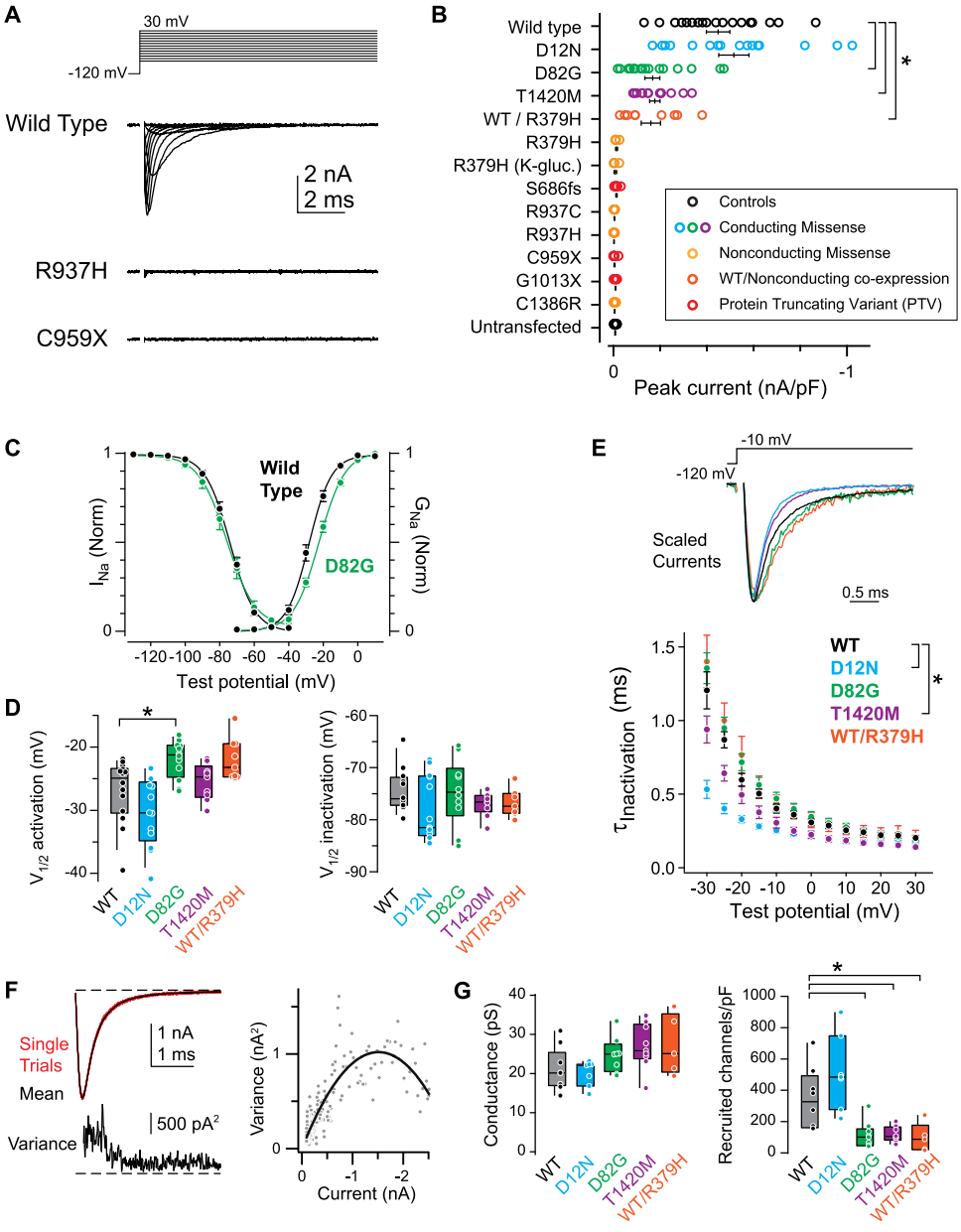

Figure 2. Electrophysiology of *SCN2A* variants. **(A)** $Na_V1.2$ activation currents from HEK293 cells transfected with wild-type (WT), C959X, and R937H plasmids. Capacitance transient blanked for clarity. Note lack of current in either variant. **(B)** Peak current amplitudes observed during activation protocol for all mutations. Data are normalized to cell capacitance and color coded to match subsequent panels (WT, black; D12N, cyan; D82G, green; T1420M, magenta; other missense, yellow; all loss of function, red). WT/R379H denotes coexpression of the two variants. R379H (K-gluc) denotes only experiments performed with a K-based internal solution. Circles are individual cells, bars are mean ± SEM. Data in yellow and red were not different than untransfected controls. *D82G, T1420M, and WT/R379H currents were smaller than WT ($p < .0006$; Kruskal-Wallis test). **(C)** Activation and inactivation curves in WT and D82G. D82G has depolarized activation. Circles and bars are mean ± SEM at each test potential. **(D)** Voltage at which half of the current was activated or inactivated for each conducting variant, compared with WT. Data shown as boxplots, with median and quartiles within the box and 10th and 90th percentiles as tails. Individual data points are overlaid as circles. *$p = .0043$ (Kruskal-Wallis test). **(E)** Top: exemplar currents from WT and conducting variants, scaled to peak. Bottom: inactivation tau determined from single exponential fit (10–90% of peak). Circles and bars are mean ± SEM. *$p < .01$ (repeated measures analysis of variance). $n = 13, 13, 10, 9$, and 6 cells for WT, D12N, D82G, T1420N, and WT/R379H, respectively. **(F)** Left top: overlay of 10 consecutive trials (black) and their average (red). Left bottom: average variance squared between individual trials and the average. Right: nonstationary fluctuation analysis was performed by comparing variance with current amplitude. Dots are individual time points, curve is parabolic fit for nonstationary fluctuation analysis. **(G)** Single-channel conductance and the number of channels contributing to the macroscopic current, as determined in panel **(F)**. Data and statistics presented as in panel **(D)**.

Thus, of the 12 ASD variants tested here, 9 (75%) resulted in a complete loss of $Na_V1.2$ conductance (Figures 1B and 2B).

We next characterized the electrophysiological properties of the three conducting missense variants. Compared with WT channels, D82G was the only variant in which the voltage dependence of channel activation was depolarized (Figure 2C; WT: –26.9 ± 1.3 mV, $n = 14$; D12N: –30.2 ± 1.5 mV, $n = 13$; D82G: –22.0 ± 0.9 mV, $n = 12$, T1420M: –25.5 ± 1.0 mV, $n = 9$; $p = .004$, WT vs. D82G only). The voltage dependence of inactivation was not altered in any variant (Figure 2D; WT: –74.3 ± 1.2 mV, $n = 12$; D12N: –78.0 ± 1.7 mV, $n = 13$; D82G: –74.8 ± 2.0 mV, $n = 10$, T1420M: –77.0 ± 0.8 mV, $n = 9$; $p > .1$, all variants vs. WT), though both D12N and T1420M currents inactivated more quickly at any given voltage (Figure 2E, e.g., τ = –30 mV; WT: 1.2 ± 0.1 ms, $n = 13$; D12N: 0.7 ± 0.1 ms, $n = 13$, $p < .001$ vs. WT; D82G: 1.4 ± 0.1 ms, $n = 10$, $p = .5$ vs. WT; T1420M: 0.9 ± 0.09 ms, $n = 9$; $p < .01$ vs. WT; repeated measures analysis of variance).

Last, we used fluctuation analysis to estimate single channel conductance and functional channel density (Figure 2F, G). Single channel conductance estimates were comparable to those obtained from recordings of single

channels (WT: 20.8 ± 1.8 pS, $n = 9$) (31) and were not affected in any variant (D12N: 20.1 ± 1.2 pS, $n = 7$; D82G: 24.8 ± 1.6 pS, $n = 8$; T1420M: 26.9 ± 1.9 pS, $n = 9$; $p > .05$, across all vs. WT); however, the number of channels contributing to currents was reduced in D82G and T1420M variants (channels/pF; WT: 345 ± 70, $n = 8$; D12N: 512 ± 91, $n = 7$, $p = .15$; D82G: 111 ± 28, $n = 9$, $p = .003$; T1420M: 118 ± 18, $n = 8$, $p = .003$, all vs. WT). Surface Na_V staining, assessed with total internal reflectance fluorescence, was similarly reduced in T1420M variants (Figure S2C, D in Supplement 1; Na_V/green fluorescent protein mean intensity, WT: 0.45 ± 0.05, $n = 13$; T1420M: 0.31 ± 0.03, $n = 13$; $p = .006$); however, no reduction was observed for D82G (0.40 ± 0.03, $n = 10$, $p = .3364$). This discrepancy between fluctuation analysis and surface expression for D82G may be due in part to the observed shift in voltage dependent activation. Because D82G channels are less effectively activated at voltages used for fluctuation analysis (see Supplement 1), a smaller fraction of surface-localized channels would contribute to the current. Overall, these results indicate that ASD-associated mutations can result in a wide range of dysfunction in $Na_V1.2$ and that all three of the conducting missense mutations tested reduced $Na_V1.2$ function (Figure 2).

Dominant negative effects of PTVs on WT channels have been reported when *SCN2A* alpha subunits are expressed in isolation; however, these effects are not present when channels are coexpressed with β subunits (32). Some have hypothesized that Na_Vs form functional complexes in the AIS whereby the activation of one channel hyperpolarizes voltage-dependent activation of its neighbors (33). Nonconducting variants may interfere with coupling between neighboring functional channels. Therefore, we coexpressed WT with the nonconducting variant R379H. While peak currents were smaller than WT alone (–160 ± 41 pA, $n = 9$, $p = .0006$), no change in voltage dependence, kinetics, or conductance were observed ($V_{1/2}$ activation: –22 ± 1.1 mV, $n = 9$, $p = .0472$ [postcorrection α required for significance: <.0167]; $V_{1/2}$ inactivation: –76.8 ± 1.0 mV, $n = 7$, $p = .227$; τ = –30 mV: 1.4 ± 0.2 ms, $n = 6$, $p = .350$; single-channel conductance: 27.2 ± 3.4 pS, $n = 5$, $p = .112$; channels/pF: 94 ± 41, $n = 5$, $p = .011$, all vs. WT). This indicates that nonconducting variants lack dominant negative effects on WT channels and suggests that $Na_V1.2$ channels do not couple functionally (6).

Multiple lines of evidence suggest that disruption in neocortical circuits can contribute to infantile seizures and ASD (3,30,32,34). To test how dysfunction in $Na_V1.2$ affects neuronal excitability, we incorporated each type of $Na_V1.2$ mutation observed into an established computational model of a cortical pyramidal cell (35). Because the mutations observed in ASD are heterozygous, we incorporated equal amounts of WT and mutated channels into the model and incorporated changes to the affected allele based on results in Figure 2 (see Supplement 1). To validate that these models accurately predict changes in neuronal excitability, and to compare ASD mutations with other conditions (Figure 1), BIFS and EE variants were also modeled. These include L1563V and L1330F, which are associated with BIFS and produce modest (~5 mV) shifts in steady-state voltage dependence (24), and E1211K and I1473M, which are associated with EE and produce larger (14–22 mV) changes in voltage dependence (23).

As pyramidal neurons are incorporating into cortical networks during early development, they express only $Na_V1.2$ in the AIS (15–17), and it is thought that *SCN2A* variants associated with BIFS produce seizures because $Na_V1.2$ plays the dominant role in neuronal excitability at this age (7). This time period may also be critical for ASD, as the early development of prefrontal layer 5/6 pyramidal cells has been implicated in the disorder (13). Therefore, we created a developmental model in which $Na_V1.2$ was expressed throughout the AIS and axon and a mature model in which $Na_V1.2$ was replaced by $Na_V1.6$ in the distal AIS and axon. In control conditions, spike threshold was depolarized in the developmental model relative to the mature model, consistent with the differences in voltage-dependent activation between the two isoforms (Figure 3; Figure S3 in Supplement 1). Intermediary developmental time points with different densities or distributions of $Na_V1.2$ versus $Na_V1.6$ were also modeled (Figure S4 in Supplement 1).

In the developmental model, BIFS variants hyperpolarized spike threshold and enhanced in spike rate, consistent with seizure phenotypes at this early age. EE variants were more excitable, firing spikes even at rest. In contrast, ASD variants were far less excitable than WT. Full PTV/nonconducting missense models had a rheobase spike threshold 7 mV more depolarized than WT conditions. Similarly, spike threshold in models of D12N, D82G, and T1420M variants was depolarized to levels comparable to a 40%–50% reduction in overall $Na_V1.2$ conductance. In all cases, spike rate was suppressed, suggesting that even though missense mutations have different effects on $Na_V1.2$ channels, they produce comparable deficits in neuronal excitability. Therefore, all 12 of the observed ASD variants were predicted to reduce the excitability of cortical pyramidal neurons during early development.

In the mature model, BIFS variants had only modest effects on threshold or spike rate, whereas EE variants still resulted in marked hyperexcitability. This is consistent with seizure resolution in BIFS, but not in EE. Interestingly, the ASD variants also resulted in minimal changes in neuronal excitability. Mature excitability developed gradually as more $Na_V1.6$ was incorporated into the AIS (Figure S4 in Supplement 1). Overall, this suggests that the critical period for *SCN2A* mutations to produce an ASD phenotype through changes in neuronal excitability occurs during early development.

DISCUSSION

Mutations in *SCN2A* are strongly associated with both ASD and infantile seizures. Here, we characterized the functional impact of all 11 de novo mutations in *SCN2A* from ASD cases in the Simons Simplex Collection and Autism Sequencing Consortium. All three PTVs (i.e., nonsense and frameshift) and the majority of missense mutations resulted in a complete loss of $Na_V1.2$ function, despite normal trafficking to the membrane (Figure 2; Figure S2 in Supplement 1). Three missense mutations—D12N, D82G, and T1420M—altered channel function in different ways. Remarkably, all 11 alterations in channel function evoked comparable deficits in neuronal excitability in pyramidal cell simulations of the developing brain (Figure 3)

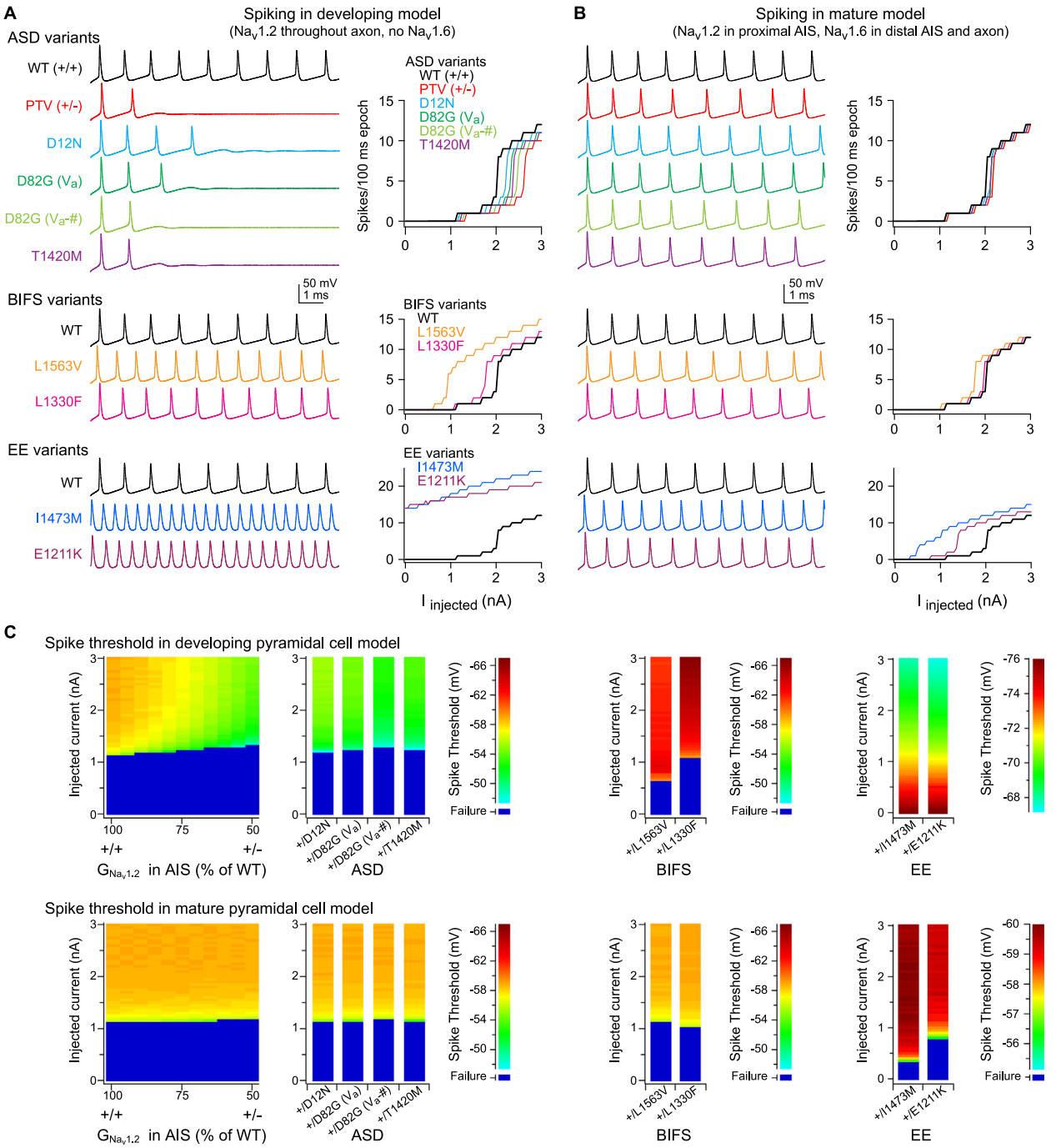

Figure 3. Neuronal excitability in a cortical pyramidal cell model. **(A)** Spiking generated with 2.2 nA somatic current in autism spectrum disorder (ASD), benign infantile familial seizures (BIFS), and epileptic encephalopathy (EE) variants. Data are modeled in a developing neuron expressing only $Na_V1.2$ in the axon initial segment (AIS) and axon. Top: all conducting ASD variants, compared with wild-type (WT) and protein-truncating variant (PTV)/nonconducting missense variants modeled as a 50% reduction in overall $Na_V1.2$ conductance. D82G was modeled as either an activation shift alone (D82G V_a) or with a reduction in channel density (D82G V_a-#). Bottom: two BIFS and two EE variants, each compared with WT. Data are vertically offset in 100-mV increments; all traces begin at –78 mV. Plots detail the number of spikes evoked in 100-ms epochs with varying somatic current injections. PTV is from 50% reduction model. Data are color coded as in legend. **(B)** Same as panel **(A)**, but in a mature pyramidal cell model, with a mix of $Na_V1.2$ and $Na_V1.6$ in the AIS, and $Na_V1.6$ in the axon (for distributions, see Figure S3 in Supplement 1). **(C)** Spike threshold with varying levels of $Na_V1.2$ in the AIS, from WT (100%) to different levels of compensation in cells heterozygous for PTV/nonconducting missense variants (to 50%) and conducting missense ASD, BIFS, and EE variants. Colored scale bar corresponds to spike threshold of the first spike observed in each trace; dark blue are conditions in which no spikes were generated. Note different scaling for EE conditions, as these variants were excitable at/near rest.

and were consistent with excitability changes observed in recordings from dissociated neurons from heterozygous *SCN2A* deficient mice (36). Thus, these results indicate that functional haploinsufficiency of *SCN2A*, generated by a variety of PTV and missense mutations, leads to substantial ASD risk.

The most common result of ASD-related missense mutation was a loss of channel conductance without dominant negative interactions. One of these mutations occurred in the outer vestibule (C1386R), an area important for channel conductance (37). Several more were observed within the pore at conserved arginine residues (R379, R937). These residues are notable, as mutations here are the only instance of two de novo missense mutations occurring at the same residue in two different families among 4,109 cases with exome data (2). Two missense mutations located on the N-terminal domain altered inactivation kinetics (D12N) and the voltage dependence of steady-state activation (D82), demonstrating, to our knowledge, the first examples of pathological N-terminal mutations in $Na_V1.2$ (38). T1420M, which is in close proximity to the pore selectivity filter (Figure 1), also had deleterious effects on channel function, increasing the speed of inactivation and reducing functional (Figure 2G) and physical channel surface density (Figure S2C, D in Supplement 1). Mutation of a homologous residue in rat $Na_V1.4$ to cysteine had modest effects on channel function (39), suggesting that the observed change in pore hydrophobicity is critical at this residue.

Because all *SCN2A* mutations analyzed led to haploinsufficiency, including all missense variants characterized here, we can revise our estimate of the contribution of *SCN2A* mutations to ASD risk. Across the 4109 ASD cases, 12 (0.29%) have mutations resulting in *SCN2A* haploinsufficiency, a figure marginally higher than that for *CHD8* (0.24% if equivalent functional analyses validated three non-PTV mutations along with the seven PTV mutations), making *SCN2A* the gene with the strongest evidence for ASD-association based on exome analysis and second only to fragile X syndrome as a single gene cause of ASD. Therefore, examination of the neurobiology consequent to *SCN2A* haploinsufficiency, alongside parallel analysis of genes related to chromatin regulation, synaptic structure, and fragile X syndrome, is likely to provide critical insights into the etiology of ASD.

Modeling ASD-associated *SCN2A* mutations in pyramidal neurons predicted a reduction in neuronal excitability in the developing brain in which $Na_V1.2$ is present throughout the AIS and axon, but minimal changes in neuronal excitability in the mature brain in which $Na_V1.2$ is restricted to the proximal AIS (Figure 3). If neuronal excitability were the main physiological consequence of reduced $Na_V1.2$ function, this would imply that the contribution of *SCN2A* mutations to the ASD phenotype occurs primarily during early development. Of note, pyramidal cortical neurons during midfetal development have previously been implicated in ASD through coexpression networks (13). Because the ASD phenotype persists in the mature brain, the decrease in neuronal excitability would need to result in a downstream change that persists after neuronal excitability returns to physiological levels. Examples of such a downstream effect include the formation and maturation of cortical circuits and the balance of excitatory and inhibitory inputs within these circuits (40,41).

Alternatively, $Na_V1.2$ dysfunction may continue to affect circuits even after these early developmental time periods in a manner not simulated in our model. APs initiated in the distal AIS propagate forward, toward axonal release sites, and backward, throughout the soma and dendrites (backpropagation). In mature pyramidal cells, $Na_V1.2$ channels in the proximal AIS are thought to provide an important electrical boost to promote effective backpropagation of APs into the somatodendritic compartment (6), and this function may still be impaired in the mature cell. Backpropagating spikes are critical signals for activity-dependent transcription, dendritic integration, and synaptic plasticity (42,43). In this way, mutations in *SCN2A* may interact with other ASD-associated mutations at the synapse (44,45), or at the transcriptional level. Thus, even though $Na_V1.2$ channels are restricted to the axon, *SCN2A* haploinsufficiency may result in cellular and circuit dysfunctions that may be common to other causes of ASD.

In contrast to ASD, the *SCN2A* variants observed in infantile seizures have a gain of function effect on $Na_V1.2$. Computational models showed that variants observed in BIFS result in increased neuronal excitability during early development, but not in the mature brain (Figure 3), consistent with the observed resolution of infantile seizures without further apparent neurological impairment (Table S1 in Supplement 2). The variants characterized in EE are predicted to result in a greater degree of neuronal excitability that persists in the mature brain (Figure 3). This is consistent with the severe seizure phenotype that often persists beyond infancy and is accompanied by profound neurological impairment from an early age (Table S1 in Supplement 2).

Numerous genetic loci associated with neuropsychiatric disorders are observed across a range of diagnoses including developmental delay, ASD, and schizophrenia. Previously, correlation between phenotype and genotype has been described for some large-scale recurrent deletions and duplications (2,46). Here, we show that functional analysis of apparently similar *SCN2A* missense mutations (Figure S1 in Supplement 1) can distinguish two neuropsychiatric phenotypes—infantile seizures and ASD/developmental delay—with further correlation between functional severity and phenotypic severity for infantile seizures (Figure 3). Thus, the specific functional effect of each *SCN2A* mutation is directly affecting the observed neuropsychiatric phenotype, presumably with genetic background, environmental influences, and stochastic effects also playing a modifying role. It remains to be seen if further functional characterization can distinguish more closely related phenotypes such as ASD and intellectual disability (Figure 1D).

While we focused on understanding $Na_V1.2$ dysfunction in cortical pyramidal cells, *SCN2A* expression in other cell types may also contribute to ASD. Though the majority of cortical interneurons express *SCN1A*/$Na_V1.1$ at the AIS (47,48), with loss of function resulting in Dravet syndrome with EE (49), somatostatin positive interneurons, which play a role in cortical circuit maturation (50,51), express a mix of both $Na_V1.1$ and $Na_V1.2$ in the proximal AIS (9). Further, $Na_V1.2$ channels are expressed throughout cerebellar granule cell axons (8), potentially contributing to episodic ataxia (25). Consequently, further functional studies, including in vivo

models expressing specific *SCN2A* variants, will be required to fully understand the pathophysiological consequences of deleterious *SCN2A* variants. Nevertheless, the comprehensive functional assessment of ASD-associated mutations alongside the existing literature on *SCN2A* variation and electrophysiology (Table S1 in Supplement 2) provides an initial insight into the genotype-phenotype correlations for this gene. The variants associated with infantile seizures lead to gain of function in $Na_V1.2$, resulting in increased neuronal excitability and the extent of the effect on neuronal excitability may explain the varying severity of this phenotype. These gain-of-function variants are usually missense variants in proximity to the voltage sensing fourth transmembrane segment and possibly in the C-terminus (Figure 1A). In contrast, our analysis shows that variants observed in ASD are usually de novo and lead to loss of function by introducing a premature stop codon (PTV) or by disrupting the pore loop and possibly the N-terminus (Figure 1B). These variants lead to loss of function in $Na_V1.2$ (Figure 2), resulting in reduced neuronal excitability during development only (Figure 3). We predict that this defect in neuronal excitability would result in a persistent change in neuronal circuitry or activity that would converge with neurobiological changes observed following disruption of ASD-associated chromatin regulating or synaptic genes.

ACKNOWLEDGMENTS AND DISCLOSURES

This work was supported by Simons Foundation Grant No. SFARI 362242 (to KJB) and National Institutes of Health Grant Nos. F32NS095580 (to RB-S) and R01 MH110928 (to SJS).

RB-S, SJS, and KJB were responsible for conceptualization; RB-S, CMK, KNB, and JYA were responsible for acquisition of data; RB-S, KNB, JYA, SJS, and KJB were responsible for data analysis; and RB-S, SJS, and KJB were responsible for writing.

We are grateful to all the families participating in this research, including the Simons Foundation Autism Research Initiative (SFARI) Simplex Collection (SSC) and the Autism Sequencing Consortium (ASC). We thank members of the Bender and Sanders labs, as well as Drs. A. Brumback, J. Rubenstein, V. Sohal, and M. State for comments.

The authors report no biomedical financial interests or potential conflicts of interest.

ARTICLE INFORMATION

From the Center for Integrative Neuroscience (RB-S, CMK, KJB), Kavli Institute for Fundamental Neuroscience, Department of Neurology; Department of Psychiatry (JYA, SJS); and UCSF Weill Institute for Neurosciences (JYA, SJS, KJB), University of California, San Francisco, San Francisco; Computational Research Division (RB-S), Lawrence Berkeley National Laboratory, Berkeley, California; and the Department of Chemistry (KNB), University of Puerto Rico, Río Piedras Campus, San Juan, Puerto Rico.

SJS and KJB contributed equally to this work.

Address correspondence to Kevin J. Bender, Ph.D., UCSF Weill Institute for Neurosciences, University of California, San Francisco, San Francisco, CA 94158; E-mail: kevin.bender@ucsf.edu.

Received Sep 26, 2016; revised Dec 14, 2016; accepted Jan 10, 2017.

Supplementary material cited in this article is available online at http://dx.doi.org/10.1016/j.biopsych.2017.01.009.

REFERENCES

1. Sanders SJ, Murtha MT, Gupta AR, Murdoch JD, Raubeson MJ, Willsey AJ, *et al*. (2012): De novo mutations revealed by whole-exome sequencing are strongly associated with autism. Nature 485:237–241.
2. Sanders SJ, He X, Willsey AJ, Ercan-Sencicek AG, Samocha KE, Cicek AE, *et al*. (2015): Insights into autism spectrum disorder genomic architecture and biology from 71 risk loci. Neuron 87: 1215–1233.
3. De Rubeis S, He X, Goldberg AP, Poultney CS, Samocha K, Cicek AE, *et al*. (2014): Synaptic, transcriptional and chromatin genes disrupted in autism. Nature 515:209–215.
4. Iossifov I, O'Roak BJ, Sanders SJ, Ronemus M, Krumm N, Levy D, *et al*. (2014): The contribution of de novo coding mutations to autism spectrum disorder. Nature 515:216–221.
5. Fitzgerald TW, Gerety SS, Jones WD, van Kogelenberg M, King DA, McRae J, *et al*. (2015): Large-scale discovery of novel genetic causes of developmental disorders. Nature 519:223–228.
6. Hu W, Tian C, Li T, Yang M, Hou H, Shu Y (2009): Distinct contributions of Na(v)1.6 and Na(v)1.2 in action potential initiation and backpropagation. Nat Neurosci 12:996–1002.
7. Liao Y, Deprez L, Maljevic S, Pitsch J, Claes L, Hristova D, *et al*. (2010): Molecular correlates of age-dependent seizures in an inherited neonatal-infantile epilepsy. Brain 133:1403–1414.
8. Martinez-Hernandez J, Ballesteros-Merino C, Fernandez-Alacid L, Nicolau JC, Aguado C, Lujan R (2013): Polarised localisation of the voltage-gated sodium channel Na(v)1.2 in cerebellar granule cells. Cerebellum 12:16–26.
9. Li T, Tian C, Scalmani P, Frassoni C, Mantegazza M, Wang Y, *et al*. (2014): Action potential initiation in neocortical inhibitory interneurons. PLoS Biol 12:e1001944.
10. Tian C, Wang K, Ke W, Guo H, Shu Y (2014): Molecular identity of axonal sodium channels in human cortical pyramidal cells. Front Cell Neurosci 8:297.
11. Howell KB, McMahon JM, Carvill GL, Tambunan D, Mackay MT, Rodriguez-Casero V, *et al*. (2015): SCN2A encephalopathy: A major cause of epilepsy of infancy with migrating focal seizures. Neurology 85:958–966.
12. Chang J, Gilman SR, Chiang AH, Sanders SJ, Vitkup D (2015): Genotype to phenotype relationships in autism spectrum disorders. Nat Neurosci 18:191–198.
13. Willsey AJ, Sanders SJ, Li M, Dong S, Tebbenkamp AT, Muhle RA, *et al*. (2013): Coexpression networks implicate human midfetal deep cortical projection neurons in the pathogenesis of autism. Cell 155: 997–1007.
14. Xu X, Wells AB, O'Brien DR, Nehorai A, Dougherty JD (2014): Cell type-specific expression analysis to identify putative cellular mechanisms for neurogenetic disorders. J Neurosci 34:1420–1431.
15. Boiko T, Van Wart A, Caldwell JH, Levinson SR, Trimmer JS, Matthews G (2003): Functional specialization of the axon initial segment by isoform-specific sodium channel targeting. J Neurosci 23: 2306–2313.
16. Gazina EV, Leaw BT, Richards KL, Wimmer VC, Kim TH, Aumann TD, *et al*. (2015): 'Neonatal' Nav1.2 reduces neuronal excitability and affects seizure susceptibility and behaviour. Hum Mol Genet 24: 1457–1468.
17. Osorio N, Alcaraz G, Padilla F, Couraud F, Delmas P, Crest M (2005): Differential targeting and functional specialization of sodium channels in cultured cerebellar granule cells. J Physiol 569:801–816.
18. Bender KJ, Trussell LO (2012): The physiology of the axon initial segment. Annu Rev Neurosci 35:249–265.
19. Kole MH, Stuart GJ (2012): Signal processing in the axon initial segment. Neuron 73:235–247.
20. Kole MH, Ilschner SU, Kampa BM, Williams SR, Ruben PC, Stuart GJ (2008): Action potential generation requires a high sodium channel density in the axon initial segment. Nat Neurosci 11:178–186.
21. Xu R, Thomas EA, Jenkins M, Gazina EV, Chiu C, Heron SE, *et al*. (2007): A childhood epilepsy mutation reveals a role for developmentally regulated splicing of a sodium channel. Mol Cell Neurosci 35: 292–301.
22. Lauxmann S, Boutry-Kryza N, Rivier C, Mueller S, Hedrich UB, Maljevic S, *et al*. (2013): An SCN2A mutation in a family with infantile seizures from Madagascar reveals an increased subthreshold Na(+) current. Epilepsia 54:e117–e121.

23. Ogiwara I, Ito K, Sawaishi Y, Osaka H, Mazaki E, Inoue I, *et al*. (2009): De novo mutations of voltage-gated sodium channel alphaII gene SCN2A in intractable epilepsies. Neurology 73:1046–1053.
24. Scalmani P, Rusconi R, Armatura E, Zara F, Avanzini G, Franceschetti S, *et al*. (2006): Effects in neocortical neurons of mutations of the Na(v) 1.2 Na+ channel causing benign familial neonatal-infantile seizures. J Neurosci 26:10100–10109.
25. Schwarz N, Hahn A, Bast T, Muller S, Loffler H, Maljevic S, *et al*. (2016): Mutations in the sodium channel gene SCN2A cause neonatal epilepsy with late-onset episodic ataxia. J Neurol 263:334–343.
26. Misra SN, Kahlig KM, George AL Jr. (2008): Impaired NaV1.2 function and reduced cell surface expression in benign familial neonatal-infantile seizures. Epilepsia 49:1535–1545.
27. Sanders SJ (2015): First glimpses of the neurobiology of autism spectrum disorder. Curr Opin Genet Dev 33:80–92.
28. Lek M, Karczewski KJ, Minikel EV, Samocha KE, Banks E, Fennell T, *et al*. (2016): Analysis of protein-coding genetic variation in 60,706 humans. Nature 536:285–291.
29. Petrovski S, Gussow AB, Wang Q, Halvorsen M, Han Y, Weir WH, *et al*. (2015): The intolerance of regulatory sequence to genetic variation predicts gene dosage sensitivity. PLoS Genet 11:e1005492.
30. Zhu G, Zhang Y, Xu H, Jiang C (1998): Identification of endogenous outward currents in the human embryonic kidney (HEK 293) cell line. J Neurosci Methods 81:73–83.
31. Stuhmer W, Methfessel C, Sakmann B, Noda M, Numa S (1987): Patch clamp characterization of sodium channels expressed from rat brain cDNA. Eur Biophys J 14:131–138.
32. Kamiya K, Kaneda M, Sugawara T, Mazaki E, Okamura N, Montal M, *et al*. (2004): A nonsense mutation of the sodium channel gene SCN2A in a patient with intractable epilepsy and mental decline. J Neurosci 24:2690–2698.
33. Naundorf B, Wolf F, Volgushev M (2006): Unique features of action potential initiation in cortical neurons. Nature 440:1060–1063.
34. Noebels J (2015): Pathway-driven discovery of epilepsy genes. Nat Neurosci 18:344–350.
35. Hallermann S, de Kock CP, Stuart GJ, Kole MH (2012): State and location dependence of action potential metabolic cost in cortical pyramidal neurons. Nat Neurosci 15:1007–1014.
36. Planells-Cases R, Caprini M, Zhang J, Rockenstein EM, Rivera RR, Murre C, *et al*. (2000): Neuronal death and perinatal lethality in voltage-gated sodium channel alpha(II)-deficient mice. Biophys J 78: 2878–2891.
37. Cervenka R, Zarrabi T, Lukacs P, Todt H (2010): The outer vestibule of the Na+ channel-toxin receptor and modulator of permeation as well as gating. Mar Drugs 8:1373–1393.
38. Sugawara T, Tsurubuchi Y, Agarwala KL, Ito M, Fukuma G, Mazaki-Miyazaki E, *et al*. (2001): A missense mutation of the Na+ channel alpha II subunit gene Na(v)1.2 in a patient with febrile and afebrile seizures causes channel dysfunction. Proc Natl Acad Sci U S A 98: 6384–6389.
39. Yamagishi T, Xiong W, Kondratiev A, Velez P, Mendez-Fitzwilliam A, Balser JR, *et al*. (2009): Novel molecular determinants in the pore region of sodium channels regulate local anesthetic binding. Mol Pharmacol 76:861–871.
40. Nelson SB, Valakh V (2015): Excitatory/inhibitory balance and circuit homeostasis in autism spectrum disorders. Neuron 87: 684–698.
41. Shepherd GM, Katz DM (2011): Synaptic microcircuit dysfunction in genetic models of neurodevelopmental disorders: Focus on Mecp2 and Met. Curr Opin Neurobiol 21:827–833.
42. Feldman DE (2012): The spike-timing dependence of plasticity. Neuron 75:556–571.
43. Saha RN, Dudek SM (2008): Action potentials: To the nucleus and beyond. Exp Biol Med (Maywood) 233:385–393.
44. Aceti M, Creson TK, Vaissiere T, Rojas C, Huang WC, Wang YX, *et al*. (2015): Syngap1 haploinsufficiency damages a postnatal critical period of pyramidal cell structural maturation linked to cortical circuit assembly. Biol Psychiatry 77:805–815.
45. Philpot BD, Thompson CE, Franco L, Williams CA (2011): Angelman syndrome: Advancing the research frontier of neurodevelopmental disorders. J Neurodev Disord 3:50–56.
46. Rees E, Walters JT, Georgieva L, Isles AR, Chambert KD, Richards AL, *et al*. (2014): Analysis of copy number variations at 15 schizophrenia-associated loci. Br J Psychiatry 204:108–114.
47. Catterall WA, Kalume F, Oakley JC (2010): NaV1.1 channels and epilepsy. J Physiol 588:1849–1859.
48. Ogiwara I, Miyamoto H, Morita N, Atapour N, Mazaki E, Inoue I, *et al*. (2007): Nav1.1 localizes to axons of parvalbumin-positive inhibitory interneurons: A circuit basis for epileptic seizures in mice carrying an Scn1a gene mutation. J Neurosci 27:5903–5914.
49. Depienne C, Trouillard O, Saint-Martin C, Gourfinkel-An I, Bouteiller D, Carpentier W, *et al*. (2009): Spectrum of SCN1A gene mutations associated with Dravet syndrome: Analysis of 333 patients. J Med Genet 46:183–191.
50. Anastasiades PG, Marques-Smith A, Lyngholm D, Lickiss T, Raffiq S, Katzel D, *et al*. (2016): GABAergic interneurons form transient layer-specific circuits in early postnatal neocortex. Nat Commun 7:10584.
51. Tuncdemir SN, Wamsley B, Stam FJ, Osakada F, Goulding M, Callaway EM, *et al*. (2016): Early somatostatin interneuron connectivity mediates the maturation of deep layer cortical circuits. Neuron 89:521–535.